Comput Mech (2009) 43:769–779
DOI 10.1007/s00466-008-0344-5

ORIGINAL PAPER

A small-strain model to simulate the curing of thermosets

M. Hossain · G. Possart · P. Steinmann

Received: 20 May 2008 / Accepted: 26 September 2008 / Published online: 22 October 2008

Abstract This contribution presents a newly developed phenomenological model to describe the curing process of thermosets undergoing small strain deformations. The governing equations are derived from a number of physical and chemical presuppositions and details of the numerical implementation within the finite element method are given. The curing of thermosets is a very complex process involving a series of chemical reactions which result in the conversion of liquid low molecular weight monomer mixtures into highly cross-linked solid macromolecular structures. This phase transition from a viscous fluid to a viscoelastic solid can be modelled by a constitutive relation which is based on a temporal evolution of shear modulus and relaxation time. Some numerical examples demonstrate the capability of the model to correctly represent the evolution of elastic and inelastic material properties as well as the volume shrinkage taking place during the curing process.

Keywords Curing · Thermosets · Viscoelasticity · Stiffness increase · Volume shrinkage

M. Hossain
Chair of Applied Mechanics, University of Kaiserslautern,
P.O. Box 3049, 67653 Kaiserslautern, Germany
e-mail: hossain@rhrk.uni-kl.de

G. Possart · P. Steinmann (✉)
Chair of Applied Mechanics, University of Erlangen-Nuremberg,
Egerlandstraße 5, 91058 Erlangen, Germany
e-mail: paul.steinmann@ltm.uni-erlangen.de

G. Possart
e-mail: gunnar.possart@ltm.uni-erlangen.de

1 Introduction

For many applications in automotive, electronics or aerospace industry, constitutive models are needed that consider time- or degree of cure dependent properties of adhesives like polyester or epoxy resins [1]. A typical application relevant for such models is the production of carbon or glass fibre-reinforced epoxy laminates or structures. Other applications in this context are the adhesive bonding of metal sheets or electronic components with conducting or isolating adhesives [2].

The uncured polymer usually behaves as a deformable viscous liquid practically incapable of sustaining any other than hydrostatic load. With time evolving, the curing reactions proceed, polymer chains cross-link to each other and the viscosity of the liquid resin and its molecular weight increase. Since the cross-linking is an exothermal reaction, the formation of the polymer network is accompanied by heat generation which results in a temperature increase causing some initial viscosity decrease. The molecular growth continues with time until a perceptible gel-like lump forms. This point, where the resin transforms from liquid to solid, is called the gel point. It can also be defined as the gel time, i.e. the period from the start of the reaction to the appearance of a soft intractable gel where 1–2% of the polymer has been cross-linked. Cross-linking leads to a decrease in specific volume in the range of about 1–10%, which is frequently denoted as curing shrinkage [2–4]. In the case of fibre-reinforced laminate structures or thin metal sheets, these temperature and shrinkage effects can lead to significant residual stresses and strains or warping phenomena. Especially warpage due to process induced residual stresses has long been recognised as a major obstacle to a cost effective manufacture of composites.

1.1 Previous works

In processes that glue electronic components to plates, shrinkage- and/or temperature-induced stresses can lead to damage or even to failure of either the adhesive layer or the whole component [2,5]. Recent research has demonstrated that a careful selection of processing parameters dramatically reduces warpage which suggests that process modelling can be a powerful tool for determining optimal curing conditions [6].

Experimental data describing the change in viscoelastic material properties during cure can be found e.g. in [7–9]. Usually, the property evolutions are measured above the gel point only, i.e. for higher degrees of cure, which is considered to be the range responsible for the emergence of residual stresses [2]. O'Brien et al. [6], for example, measured the viscoelastic behaviour also below the gel point, i.e. for curing degrees in the whole range between 0 and 1.

Only limited references of models for the evolution of viscoelastic properties during thermoset curing are available in the literature. Some efforts were focused on the development of relations between viscoelastic properties and specific polymer parameters such as molecular weight, molecular weight distribution or degree of chain branching, e.g. [6]. Approaches to model the underlying curing processes [3,4,10–13] mainly deal with the residual stress build-up in polymer composites during curing and usually consider only linear elasticity or viscoelasticity. Only the recent treatments of Lion and Höfer [2] and Adolf and Chambers [14] attempt to develop general purpose continuum approaches accounting for the evolution of properties within curing polymers.

The course of dynamic mechanical properties during cure can be found in [4,9,15–17]. Fairly comprehensive reviews of different phenomenological models for the evolution of the degree of cure are given e.g. in [18,19].

Kiasat [3] developed a curing model for small strain deformations ignoring thermal effects, which have later been addressed by the same group [20]. One of the main assumptions of Kiasat is that the formation of new cross-links during curing does not affect the current stress state caused by previously applied strains, i.e. new cross-links form unstrained and stress-free.

Another approach for thermoset curing has been developed in a series of papers by Adolf and co-workers [21–24] who proposed not only linear constitutive models but also a model for large strains. Their continuum model, originally devised for viscoelastic glassy polymers, is extended towards the curing of polymers. Merely a consideration of temperature effects and volume-shrinkage during cure is not included.

Very recently, Lion and Höfer [2] proposed a phenomenological thermo-viscoelastic curing model for finite strains. It accounts for thermally and chemically induced volume changes via a ternary multiplicative split of the deformation gradient into mechanical, thermal and chemical parts. Furthermore, a coordinate of reaction is introduced corresponding to the degree of cure. The model is mainly based on the assumption of process dependent viscosities as in previous works of Haupt and Lion [25–27]. The resulting constitutive relation is claimed to be thermodynamically consistent, i.e. it fulfills the second law of thermodynamics, an issue that most of the earlier curing models did not touch.

1.2 Concepts and outline

From a rheological point of view the cross-linking process can be considered as a continuous increase in stiffness. From a molecular point of view we can assume that when a step in strain is applied, the chains between cross-links are deformed which leads to stresses in the material. Due to the progress in reaction, new cross-links are generated which will later be conceptualised by the addition of new chains to the network. These fit into the already deformed structure and are not affected by the previous deformation, i.e. new chains do not contribute to the stress until the deformation is changed. Concerning the viscous properties, curing yields increasing relaxation time and viscosity due to the fact that the newly emerging cross-links hinder molecular motions and prevent the relocation of network segments which would be responsible for stress relaxation.

The here proposed phenomenological viscoelastic curing model entirely reproduces the above mentioned aspects of thermoset cure, except for thermally induced effects which will be treated in a forthcoming work. The model is restricted to the viscoelastic stress evolution beyond the gel point since that is the most significant phase for practical applications.

This paper is organized as follows: Sect. 2 derives basic one-dimensional equations from simple rheological considerations. The simplified equations accounting for continuous stiffness gain are then extended to three-dimensions in Sect. 3. Next, a one-dimensional viscoelastic model is developed, followed again by an extension to three-dimensions (Sects. 4, 5) and a model incoporating the phenomenon of curing shrinkage (Sect. 6). Section 7 discusses the cure-dependent material parameter evolution which is followed by a final section presenting some numerical examples.

2 One-dimensional elastic curing model

In rheology, linear elastic materials can be modelled using networks of linear springs having a modulus c and responding with a stress $\sigma = c\Delta\varepsilon$ when sustaining a strain increment $\Delta\varepsilon$. Using this analogy, the onward cross-linking within a curing polymer can be conceptualised as the addition of further springs to the network, cf. Fig. 1. The stress development

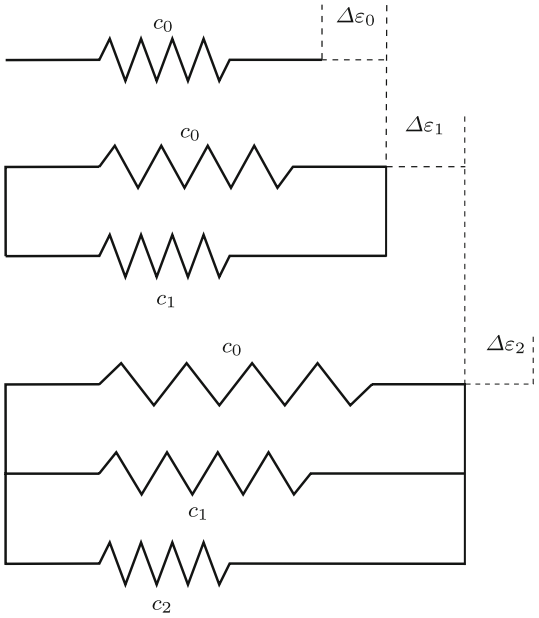

Fig. 1 One-dimensional elastic curing model: stiffness gain by adding springs

$\sigma(t_i)$ during continuous addition of elastic chains or springs c_i in-between consecutive strain increments $\Delta\varepsilon_i$ at time t_i can be written as follows:

- one spring c_0 at t_0 after strain increment $\Delta\varepsilon_0$:

  $$\sigma(t_0) = c_0 \Delta\varepsilon_0$$

- add 2nd spring and apply strain increment $\Delta\varepsilon_1$:

  $$\sigma(t_1) = c_0 \Delta\varepsilon_0 + [c_0 + c_1]\,\Delta\varepsilon_1,$$

  i.e. the first spring responds to both strain increments $\Delta\varepsilon_0 + \Delta\varepsilon_1$ while the second spring only sustains the new deformation $\Delta\varepsilon_1$.
- add 3rd spring and apply strain increment $\Delta\varepsilon_2$:

  $$\sigma(t_2) = c_0 \Delta\varepsilon_0 + [c_0 + c_1]\,\Delta\varepsilon_1 + [c_0 + c_1 + c_2]\,\Delta\varepsilon_2$$

- nth spring and nth strain increment:

$$\sigma(t_n) = \sum_{i=0}^{n} c_i \sum_{j=i}^{n} \Delta\varepsilon_j. \tag{1}$$

To obtain a continuous formulation of this discrete stress-strain relation, we define the discrete modulus updates c_i and strain increments $\Delta\varepsilon_i$ to be definite time integrals of some prescribed continuous modulus evolution $\dot{c}$ and strain history $\dot{\varepsilon}$ as

$$\Delta\varepsilon_0 = \int_0^{t_0} \dot{\varepsilon}(\tau)d\tau\,, \quad \Delta\varepsilon_i = \int_{t_{i-1}}^{t_i} \dot{\varepsilon}(\tau)d\tau$$

$$c_0 = \int_0^{t_0} \dot{c}(\tau)d\tau\,, \quad c_i = \int_{t_{i-1}}^{t_i} \dot{c}(\tau)d\tau\,.$$

Now, the continuous limit of Eq. (1) reads

$$\sigma(t) = \int_0^t \dot{c}(\tau) \int_\tau^t \dot{\varepsilon}(\bar{\tau})d\bar{\tau}d\tau. \tag{2}$$

Note that this relation reproduces the physical observation that a curing material sustaining no current change of deformation, i.e. $\dot{\varepsilon}(t) = 0$, does not change its stress state as resulted from previous deformations—even though its material properties continue to evolve. Just by the time the deformation state is changed again, the material properties evolved meanwhile define the new stress state.

Equation (2) could now be solved numerically for given parameter evolutions $\dot{c}$ and strain histories $\dot{\varepsilon}$ using suitable integration schemes, e.g. the mid-point rule:

$$\sigma(t) = \sum_{i=1}^{N}\sum_{j=i}^{N} \dot{c}(\tau_i)\left[\tau_{i+1} - \tau_i\right]\dot{\varepsilon}(\bar{\tau}_j)\left[\bar{\tau}_{j+1} - \bar{\tau}_j\right].$$

This equation is rather cumbersome to handle numerically and also difficult to extend to three-dimensions, i.e. some simplifications are desirable. From (2) we easily find

$$\begin{aligned}
\sigma(t) &= \int_0^t \dot{c}(\tau) \int_\tau^t \dot{\varepsilon}(\bar{\tau})d\bar{\tau}d\tau \\
&= \int_0^t \dot{c}(\tau)\left[\varepsilon(t) - \varepsilon(\tau)\right]d\tau \\
&= \varepsilon(t)\int_0^t \dot{c}(\tau)d\tau - \int_0^t \dot{c}(\tau)\varepsilon(\tau)d\tau \\
&= c(t)\varepsilon(t) - \int_0^t \dot{c}(\tau)\varepsilon(\tau)d\tau \\
&= c(t)\varepsilon(t) - \int_0^t \left[\dot{\overline{c(\tau)\varepsilon(\tau)}} - c(\tau)\dot{\varepsilon}(\tau)\right]d\tau \\
&= c(t)\varepsilon(t) - \int_0^t \dot{\overline{c(\tau)\varepsilon(\tau)}}d\tau + \int_0^t c(\tau)\dot{\varepsilon}(\tau)d\tau \\
&= c(t)\varepsilon(t) - c(t)\varepsilon(t) + \int_0^t c(\tau)\dot{\varepsilon}(\tau)d\tau,
\end{aligned}$$

which yields finally

$$\sigma(t) = \int_0^t c(\tau)\dot{\varepsilon}(\tau)d\tau \tag{3}$$

$$\Rightarrow \quad \dot{\sigma}(t) = c(t)\dot{\varepsilon}(t), \tag{4}$$

coinciding with the one-dimensional elastic curing model of Adolf and Gillen, cf. [14,28]. This reformulation (4) can now easily be solved using implicit integration schemes like Euler-backward:

$$\frac{\sigma^{n+1} - \sigma^n}{\Delta t} = c^{n+1}\frac{\varepsilon^{n+1} - \varepsilon^n}{\Delta t}, \tag{5}$$

where $[\bullet]^i = [\bullet](t_i)$ and $\Delta t = t_{n+1} - t_n$. Thus, for a given modulus evolution and strain history, the current stress during cure is updated according to

$$\sigma^{n+1} = \sigma^n + c^{n+1}\left[\varepsilon^{n+1} - \varepsilon^n\right]. \tag{6}$$

Calculating the derivative of σ^{n+1} with respect to the current strain ε^{n+1} yields, as expected, the current tangent operator, i.e. the accumulated modulus:

$$\frac{\partial\sigma^{n+1}}{\partial\varepsilon^{n+1}} = c^{n+1} = \int_0^{t_{n+1}} \dot{c}(\tau)d\tau. \tag{7}$$

3 Three-dimensional elastic curing model

The one-dimensional curing model discussed in the previous section is now extended to three-dimensions. We follow a frequently used assumption of isotropic polymer modelling and consider an additive split of the total stress tensor into volumetric, i.e. shape preserving, and isochoric, i.e. volume preserving and shape changing parts reading as

$$\boldsymbol{\sigma} = \boldsymbol{\sigma}_{\mathrm{vol}} + \boldsymbol{\sigma}_{\mathrm{iso}}. \tag{8}$$

Due to the curing progress both summands are again time-dependent and can, in analogy to the one-dimensional case (3), be expressed as integrals of parameter evolution times strain history

$$\boldsymbol{\sigma}_{\mathrm{vol}}(t) = \int_0^t \kappa(\tau)\,\mathrm{tr}(\dot{\boldsymbol{\varepsilon}}(\tau))\boldsymbol{I}\,d\tau \tag{9}$$

$$\boldsymbol{\sigma}_{\mathrm{iso}}(t) = 2\int_0^t \mu(\tau)\,\dot{\boldsymbol{e}}(\tau)\,d\tau, \tag{10}$$

where the volumetric part is governed by the bulk modulus evolution $\kappa(t)$ and responds only to the trace of the strain rate tensor $\mathrm{tr}(\dot{\boldsymbol{\varepsilon}}) = \dot{\varepsilon}_{ii}$, whereas the isochoric part follows a prescribed evolution of the shear modulus $\mu(t)$ and depends on the rate of the deviatoric strain tensor $\boldsymbol{e} := \mathrm{dev}(\boldsymbol{\varepsilon}) = \boldsymbol{\varepsilon} - \frac{1}{3}\mathrm{tr}(\boldsymbol{\varepsilon})\boldsymbol{I}$. By $\boldsymbol{I}$ we denote the second-order unit tensor $(\boldsymbol{I})_{ij} = \delta_{ij}$, δ_{ij} being the Kronecker symbol. As before one obtains

$$\dot{\boldsymbol{\sigma}}_{\mathrm{vol}}(t) = \kappa(t)\,\mathrm{tr}(\dot{\boldsymbol{\varepsilon}}(t))\boldsymbol{I}, \quad \dot{\boldsymbol{\sigma}}_{\mathrm{iso}}(t) = 2\mu(t)\,\dot{\boldsymbol{e}}(t),$$

which can numerically be solved using Euler-backward integration yielding the following updates for volumetric and isochoric stresses:

$$\boldsymbol{\sigma}_{\mathrm{vol}}^{n+1} = \boldsymbol{\sigma}_{\mathrm{vol}}^{n} + \kappa^{n+1}\left[\mathrm{tr}(\boldsymbol{\varepsilon}^{n+1}) - \mathrm{tr}(\boldsymbol{\varepsilon}^{n})\right]\boldsymbol{I} \tag{11}$$

$$\boldsymbol{\sigma}_{\mathrm{iso}}^{n+1} = \boldsymbol{\sigma}_{\mathrm{iso}}^{n} + 2\mu^{n+1}\left[\boldsymbol{e}^{n+1} - \boldsymbol{e}^{n}\right]. \tag{12}$$

The current total stress according to (8) reads now:

$$\boldsymbol{\sigma}^{n+1} = \boldsymbol{\sigma}^{n} + \kappa^{n+1}\left[\mathrm{tr}(\boldsymbol{\varepsilon}^{n+1}) - \mathrm{tr}(\boldsymbol{\varepsilon}^{n})\right]\boldsymbol{I} \ \ldots + 2\mu^{n+1}\left[\boldsymbol{e}^{n+1} - \boldsymbol{e}^{n}\right]. \tag{13}$$

The fourth-order tangent operator, which is crucial for the finite-element solution of boundary value problems within iterative Newton–Raphson schemes, is again obtained as the derivative of the current stress with respect to the current strain

$$\mathbb{C}^{n+1} = \frac{\partial\boldsymbol{\sigma}^{n+1}}{\partial\boldsymbol{\varepsilon}^{n+1}} = \frac{\partial\boldsymbol{\sigma}_{\mathrm{vol}}^{n+1}}{\partial\boldsymbol{\varepsilon}^{n+1}} + \frac{\partial\boldsymbol{\sigma}_{\mathrm{iso}}^{n+1}}{\partial\boldsymbol{\varepsilon}^{n+1}} =: \mathbb{C}_{\mathrm{vol}}^{n+1} + \mathbb{C}_{\mathrm{iso}}^{n+1}. \tag{14}$$

From (11) and (12) we derive

$$\mathbb{C}_{\mathrm{vol}}^{n+1} = \kappa^{n+1}\,\boldsymbol{I}\otimes\boldsymbol{I} \tag{15}$$

$$\mathbb{C}_{\mathrm{iso}}^{n+1} = 2\mu^{n+1}\left[\mathbb{I}^{\mathrm{sym}} - \frac{1}{3}\boldsymbol{I}\otimes\boldsymbol{I}\right],$$

where $\mathbb{I}^{\mathrm{sym}} = \frac{1}{2}\left[\delta_{ik}\delta_{jl} + \delta_{il}\delta_{jk}\right]$ is the symmetric fourth order identity tensor and $(\boldsymbol{A}\otimes\boldsymbol{B})_{ijkl} = A_{ij}B_{kl}$ denotes the dyadic product of second order tensors.

4 One-dimensional viscoelastic curing model

The elastic curing model introduced in Sect. 2 will now be amended by viscous behaviour. To this extent, the rheological standard model for a viscoelastic solid consisting of a parallel connection of a Maxwell- and a Hooke-element is considered [29]. To reproduce both the stiffness gain and the increase in relaxation time during curing, the viscosity of the dashpot and the parameter of the parallel spring are assumed to evolve with curing time as depicted in Fig. 2, where the arrows at spring and dashpot are introduced to indicate the cure-dependence. The spring in the Maxwell element is set to behave time-independent.

The total viscoelastic stress can be divided into equilibrium and non-equilibrium parts, representing the two

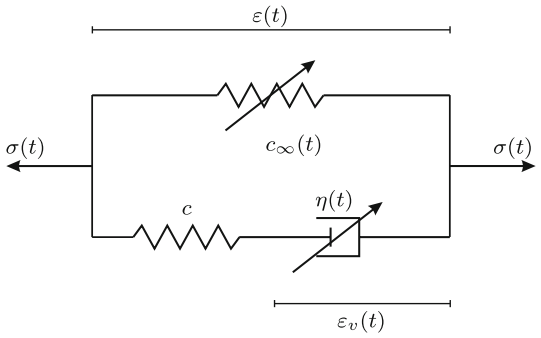

Fig. 2 One-dimensional viscoelastic curing model

contributions of the Hooke- and the Maxwell-element, respectively:

$$\sigma(t) = \sigma_{\text{eq}}(t) + \sigma_{\text{neq}}(t). \tag{16}$$

Note that, different to classic viscoelasticity, both contributions depend on time now, not only the non-equilibrium part. As in the elastic case (4), the equilibrium stress is calculated as

$$\dot{\sigma}_{\text{eq}}(t) = c_\infty(t)\dot{\varepsilon}(t), \tag{17}$$

where $c_\infty(t)$ denotes the cure-dependent equilibrium modulus and Euler-backward integration yields the update equation

$$\sigma_{\text{eq}}^{n+1} = \sigma_{\text{eq}}^{n} + c_\infty^{n+1}\left[\varepsilon^{n+1} - \varepsilon^{n}\right]. \tag{18}$$

For the dashpot we apply the standard formulation linearly relating the stress to the strain rate in terms of the viscosity. From the kinematics, cf. Fig. 2, the non-equilibrium stress is obtained to be

$$\sigma_{\text{neq}}(t) = c\left[\varepsilon(t) - \varepsilon_v(t)\right] = \eta(t)\dot{\varepsilon}_v(t), \tag{19}$$

where c and $\eta(t)$ denote the constant non-equilibrium modulus of the second spring and the cure-dependent viscosity, respectively. Rearranging $(19)_2$ yields the necessary evolution equation for the strain-like internal variable ε_v, i.e. the dashpot deformation:

$$\dot{\varepsilon}_v(t) = \frac{1}{T(t)}\left[\varepsilon(t) - \varepsilon_v(t)\right], \tag{20}$$

where the relaxation time $T(t) := \frac{\eta(t)}{c}$ has been introduced. Again by Euler-backward, the internal variable can be updated iteratively according to

$$\varepsilon_v^{n+1} = \frac{\delta^{n+1}\varepsilon^{n+1} + \varepsilon_v^{n}}{1 + \delta^{n+1}} \tag{21}$$

with the abbreviation $\delta^{n+1} = \frac{\Delta t}{T^{n+1}}$ combining relaxation time and time interval length. Now, inserting (18) and $(19)_1$ into (16) and exploiting (21) yields the final stress update equation for one-dimensional viscoelastic curing:

$$\begin{aligned}\sigma^{n+1} &= \sigma_{\text{eq}}^{n+1} + \sigma_{\text{neq}}^{n+1}\\ &= \sigma_{\text{eq}}^{n} + c_\infty^{n+1}\left[\varepsilon^{n+1} - \varepsilon^{n}\right] + c\left[\varepsilon^{n+1} - \varepsilon_v^{n+1}\right]\\ &= \sigma_{\text{eq}}^{n} + c_\infty^{n+1}\left[\varepsilon^{n+1} - \varepsilon^{n}\right] + c_\star^{n+1}\left[\varepsilon^{n+1} - \varepsilon_v^{n}\right],\end{aligned} \tag{22}$$

with $c_\star^{n+1} = \frac{c}{1+\delta^{n+1}}$, i.e. both prescribed temporal evolutions of equilibrium modulus and relaxation time as well as the previous value of the internal variable are required.

The current viscoelastic tangent operator becomes

$$\frac{\partial\sigma^{n+1}}{\partial\varepsilon^{n+1}} = c_\infty^{n+1} + \frac{c\,T^{n+1}}{T^{n+1} + \Delta t}. \tag{23}$$

5 Three-dimensional viscoelastic curing model

In analogy to the elastic case, the one-dimensional viscoelastic curing model of the previous section is now extended to three-dimensions. The total stress is again splitted into volumetric and isochoric parts

$$\boldsymbol{\sigma}(t) = \boldsymbol{\sigma}_{\text{vol}}(t) + \boldsymbol{\sigma}_{\text{iso}}(t), \tag{24}$$

where the former is handled exactly as in the elastic case (9) and (11):

$$\begin{aligned}\boldsymbol{\sigma}_{\text{vol}}(t) &= \int_0^t \kappa(\tau)\,\text{tr}\left(\dot{\boldsymbol{\varepsilon}}(\tau)\right)\boldsymbol{I}\,d\tau\\ \boldsymbol{\sigma}_{\text{vol}}^{n+1} &= \boldsymbol{\sigma}_{\text{vol}}^{n} + \kappa^{n+1}\left[\text{tr}(\boldsymbol{\varepsilon}^{n+1}) - \text{tr}(\boldsymbol{\varepsilon}^{n})\right]\boldsymbol{I}.\end{aligned} \tag{25}$$

Furthermore, all viscous effects are assumed to be purely deviatoric and the isochoric stress can again be divided into equilibrium and non-equilibrium contributions:

$$\boldsymbol{\sigma}_{\text{iso}}(t) = \boldsymbol{\sigma}_{\text{iso,eq}}(t) + \boldsymbol{\sigma}_{\text{iso,neq}}(t). \tag{26}$$

The isochoric equilibrium part is modelled identical to the elastic case (10) and (12), i.e.

$$\begin{aligned}\boldsymbol{\sigma}_{\text{iso,eq}}(t) &= 2\int_0^t \mu_\infty(\tau)\dot{\boldsymbol{e}}(\tau)d\tau\\ \boldsymbol{\sigma}_{\text{iso,eq}}^{n+1} &= \boldsymbol{\sigma}_{\text{iso,eq}}^{n} + 2\mu_\infty^{n+1}\left[\boldsymbol{e}^{n+1} - \boldsymbol{e}^{n}\right],\end{aligned} \tag{27}$$

where $\mu_\infty(t)$ denotes the equilibrium shear modulus evolution and $\boldsymbol{e} = \text{dev}\boldsymbol{\varepsilon}$ is again the deviatoric strain tensor.

The isochoric non-equilibrium stress is formulated in analogy to the one-dimensional viscoelastic case as

$$\boldsymbol{\sigma}_{\text{iso,neq}}(t) = 2\mu\left[\boldsymbol{e}(t) - \boldsymbol{e}_v(t)\right] = \eta(t)\dot{\boldsymbol{e}}_v(t), \tag{28}$$

including the constant non-equilibrium shear modulus μ and the cure-dependent viscosity evolution $\eta(t)$. From this, the evolution equation for the tensor-valued strain-like internal variable $\boldsymbol{e}_v$ follows to be

$$\dot{\boldsymbol{e}}_v(t) = \frac{1}{T(t)}\left[\boldsymbol{e}(t) - \boldsymbol{e}_v(t)\right], \tag{29}$$

where the relaxation time now reads $T(t) = \frac{\eta(t)}{2\mu}$. As before, Euler-backward scheme yields the discrete update for $\boldsymbol{e}_v$, again with $\delta^{n+1} = \frac{\Delta t}{T^{n+1}}$:

$$\boldsymbol{e}_v^{n+1} = \frac{\delta^{n+1}\boldsymbol{e}^{n+1} + \boldsymbol{e}_v^n}{1+\delta^{n+1}}. \tag{30}$$

From inserting (27) and $(28)_1$ with (30) in (26) we finally obtain the discrete update of the isochoric stress

$$\begin{aligned}\boldsymbol{\sigma}_{\text{iso}}^{n+1} &= \boldsymbol{\sigma}_{\text{iso,eq}}^{n+1} + \boldsymbol{\sigma}_{\text{iso,neq}}^{n+1} \\ &= \boldsymbol{\sigma}_{\text{iso,eq}}^{n} + 2\mu_\infty^{n+1}\left[\boldsymbol{e}^{n+1} - \boldsymbol{e}^{n}\right]\ldots \\ &\quad + 2\mu_\star^{n+1}\left[\boldsymbol{e}^{n+1} - \boldsymbol{e}_v^{n}\right],\end{aligned} \tag{31}$$

where $\mu_\star^{n+1} = \frac{\mu}{1+\delta^{n+1}}$ has been introduced.

The three-dimensional viscoelastic curing model is concluded by the discrete tangent operator:

$$\begin{aligned}\mathbb{C}_{\text{vol}}^{n+1} &= \frac{\partial \boldsymbol{\sigma}_{\text{vol}}^{n+1}}{\partial \boldsymbol{\varepsilon}^{n+1}} = \kappa^{n+1}\boldsymbol{I}\otimes\boldsymbol{I} \\ \mathbb{C}_{\text{iso}}^{n+1} &= \frac{\partial \boldsymbol{\sigma}_{\text{iso}}^{n+1}}{\partial \boldsymbol{\varepsilon}^{n+1}} = 2\left[\mu_\star^{n+1} + \mu_\infty^{n+1}\right]\left[\mathbb{I}^{\text{sym}} - \frac{1}{3}\boldsymbol{I}\otimes\boldsymbol{I}\right].\end{aligned} \tag{32}$$

6 The modelling of curing shrinkage

An important property of thermosets is the occurence of a volume reduction during polymerisation [3,30]. The formation of chemical cross-links between molecules allows them to approach much closer than in the non-bond situation leading to a more dense packing. Thus, assuming constant mass, the polymerisation progress causes a density increase. The volume shrink can take values up to 10% and, therefore, is responsible for possibly significant tensile stresses within specimen held at constant length during cure.

To incorporate this phenomenon into the curing models developed above, we introduce a new rheological element, cf. Fig. 3, which shrinks during the curing process.

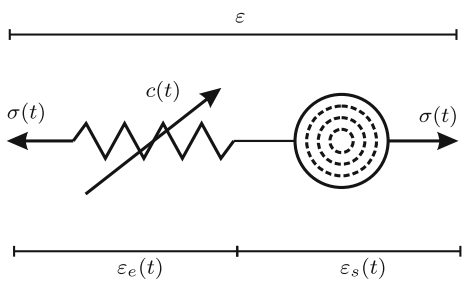

Fig. 3 One-dimensional model of curing shrinkage

Connected in series to a spring the overall response can be considered to be inverse/identical to that of a Maxwell element under tension/compression. The deformation of a dashpot under external load will, according to evolution equations like (20), increase from zero to some positive value. This reduces the elongation of the attached spring and causes stress relaxation due to the dissipation of strain energy. Vice versa, the new element shrinks from initially zero extension $\varepsilon_s^0 = 0$ to some time-dependent and negative value $\varepsilon_s^\infty < \varepsilon_s^0$. For some prescribed tension/compression this enforces an increase/decrease of the deformation of the attached elastic spring and results in higher/lower absolute stress values. The work done by the shrinkage element while deforming the spring could be considered as balanced with the release of chemical energy by the cross-linking reactions. From the one-dimensional curing model (4) the kinematics lead to

$$\dot{\sigma}(t) = c(t)\dot{\varepsilon}_e(t) = c(t)\left[\dot{\varepsilon}(t) - \dot{\varepsilon}_s(t)\right], \tag{33}$$

i.e. we account for the curing shrinkage and the stress it induces by superposition of the current strain rate with a time-dependent negative strain rate. The corresponding stress update of this one-dimensional shrinkage model reads

$$\sigma^{n+1} = \sigma^n + c^{n+1}\left[\varepsilon^{n+1} - \varepsilon^n - \varepsilon_s^{n+1} + \varepsilon_s^n\right]. \tag{34}$$

To complete the model appropriate constitutive relations for the shrinkage strain evolution $\varepsilon_s(t)$ are required. Within the literature [3] expressions like

$$\varepsilon_s(t) = p_1 \exp\left(-\left(\frac{p_2}{t}\right)^{p_3}\right) + p_4 \exp\left(-\left(\frac{p_5}{t}\right)^{p_6}\right) \tag{35}$$

are applied, where the parameters p_i have to be derived from fitting (35) to experimental data. For methods to measure the volumetric shrinkage during curing we refer to Chap. 3 of Kiasat's dissertation [3]. Figure 4 displays the shape of the shrinkage strain evolution for a particular parameter set taken from there.

The extension towards a three-dimensional cure-dependent shrinkage model is now straightforward. On a macroscopic scale it is physically reasonable to assume

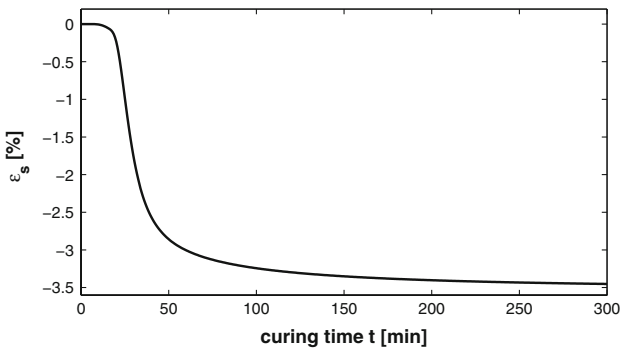

Fig. 4 Evolution of shrinkage strain

isotropic and purely volumetric shrinkage, i.e. it is sufficient to extend only the equations for the volumetric stress update of both the elastic and viscoelastic curing model. Thus, Eqs. (11)/(25) accounting for curing shrinkage read

$$\boldsymbol{\sigma}_{\mathrm{vol}}^{n+1} = \boldsymbol{\sigma}_{\mathrm{vol}}^{n} + \kappa^{n+1}\left[\mathrm{tr}\left(\boldsymbol{\varepsilon}^{n+1}\right) - \varepsilon_s^{n+1}\right]\boldsymbol{I} \ \ldots \\ - \kappa^{n+1}\left[\mathrm{tr}\left(\boldsymbol{\varepsilon}^{n}\right) - \varepsilon_s^{n}\right]\boldsymbol{I}. \tag{36}$$

Since the shrinkage strain is independent of the current strain state, both the elastic $(15)_1$ and viscoelastic $(32)_1$ volumetric tangent operators do not change.

7 Cure-dependent material parameters

This section discusses the general format of the time-/cure-dependent evolution equations of the governing material parameters that have been introduced in the previous modelling sections.

7.1 Cure-dependent shear modulus

The dependence of the shear modulus on curing can easily be investigated experimentally after the gel point. O'Brien et al. [6] also proved the cure dependent shear modulus being measurable over the entire range of cure $\alpha = 0 \ldots 1$. From the literature [7] it is known that, after the gel point, the shear modulus increases drastically following an exponential saturation function of decreasing slope until the fully cured state is reached. Thus, a simple expression for the shear modulus evolution may be

$$\mu(t) = \mu_0 + [\mu_\infty - \mu_0]\left[1 - \exp\left(-\kappa_\mu t\right)\right], \tag{37}$$

where μ_0, μ_∞ are the shear moduli at the uncured and fully cured states, respectively, and κ_μ controls the curvature, i.e. the stiffness gain velocity, cf. Fig. 5.

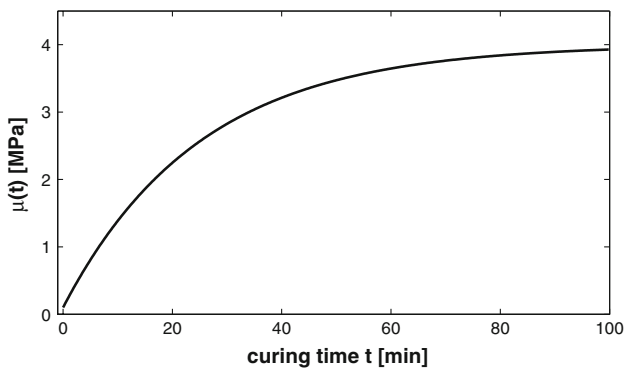

Fig. 5 Shear modulus evolution, $[\mu_0, \mu_\infty, \kappa_\mu] = [0.1, 4, 0.04]$

7.2 Cure-dependent relaxation time

The relaxation time depends both on the resin temperature and the degree of cure. The restriction of molecular motions due to the cross-linking leads to an increase in relaxation time, which is similar to the behaviour observable at a temperature decrease or, in case of dynamic loading, to a strain rate step-up. Also, a single relaxation time is typically insufficient to correctly represent the whole viscoelastic spectrum of real polymers [15]. Nonetheless, at first we restrict ourselves to only one relaxation time evolution and assume again the format of an exponential saturation function as for the shear modulus:

$$T(t) = T_0 + [T_\infty - T_0]\left[1 - \exp\left(-\kappa_\tau t\right)\right], \tag{38}$$

where T_0, T_∞ are the relaxation times at start and end of curing, respectively, and κ_τ describes the reduction rate of the viscosity.

7.3 Cure-dependent Poisson's ratio

According to the experimental observations of Kiasat [3], Poisson's ratio increases with progressive cross-linking, a behaviour also shown for temperature increases. Especially for elastomeric materials one can assume that the uncured solution is quasi-incompressible ($\nu \approx 0.5$) due to its liquid character which is followed by a slight decrease after the gel point and another increase to ≈ 0.5 after reaching the rubbery plateau. Since there are only few experimental results for the evolution of Poisson's ratio of thermosets we follow O'Brien et al. [6] approach of a constant ν, an assumption additionally justified by the lack of rubber-like characteristics of thermosets and the relatively minor influence that changes in Poisson's ratio have on the shear modulus.

7.4 Cure-dependent bulk modulus

The bulk modulus, i.e. the volumetric stress evolves similarly to the isochoric stiffness gain during cure. Due to the assumption of constant Poisson's ratio the bulk modulus evolution can be coupled to the shear modulus evolution by exploiting

$$\kappa = \frac{2\mu(1+\nu)}{3(1-\nu)}, \tag{39}$$

which is valid for linear isotropic material. Thus, the current bulk modulus $\kappa(t)$ is calculated here from

$$\kappa(t) = \frac{2\mu(t)(1+\nu)}{3(1-\nu)}. \tag{40}$$

7.5 Degree of cure/degree of polymerisation

Instead of utilising parameter evolutions formulated in terms of isothermal curing time, one could also employ formula-

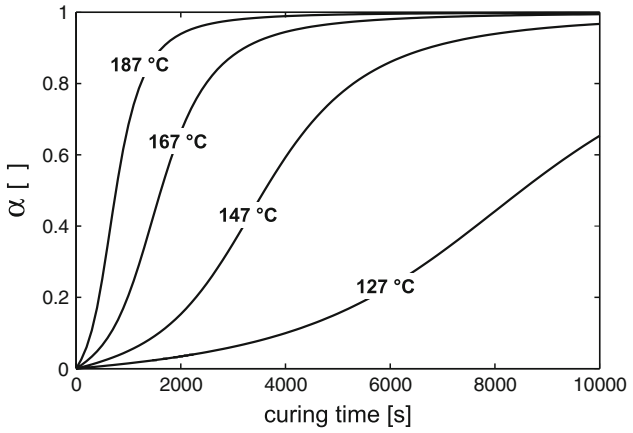

Fig. 6 Curing progress versus temperature, Kamal model

tions relating the current material parameters to the so-called degree/extent of cure α, a quantity defined by

$$\alpha(t) = \frac{H(t)}{H_{\max}} \in [0, 1], \tag{41}$$

where $H(t)$ denotes the amount of heat released by the cross-linking reactions until time t and $H_{\max}$ is the total isothermal polymerisation heat. This approach has the advantage that physical and chemical quantities like temperature or activation energies as well as their temporal evolutions are directly connected to current constitutive parameters. For this case, the time-dependence of material properties would be included implicitly via α, e.g. by $\mu = \mu(\alpha(t))$ for the shear modulus. For the sake of simplicity we will here concentrate on directly time-dependent parameter sets.

Several phenomenological models for calculating the degree of cure α have been proposed in the literature, see e.g. [2,15,18,19,31]. A frequently used kinetic model for isothermal curing of epoxy resins, the so-called autocatalytic or Kamal's model, reads

$$\frac{d\alpha}{dt} = [k_1 + k_2\alpha^m][1-\alpha]^n, \tag{42}$$

where $k_i = A_i \exp(-E_i/R\Theta)$ are temperature dependent reaction rates following an Arrhenius relationship, A_i, E_i denote frequency factors and activation energies, Θ, R are curing temperature and universal gas constant and m, n represent the reaction orders, respectively. Figure 6 displays the curing kinetics according to (42) for different temperatures based on data taken from Karkanas et al. [19].

8 Numerical examples

A number of numerical examples is presented within this section to demonstrate that the proposed models are appropriate to correctly reproduce the mechanical behaviour of thermosets during isothermal cure. The stiffness gain as well as the strain rate dependence of the stress response are shown to be realised by both the elastic and viscoelastic models. All simulations have been computed using an in-house finite element tool that has been extended by the constitutive equations and tangent operators given in Sects. 3 and 5. The one-dimensional examples reflect the behaviour of a single eight-noded hex-element for some prescribed uniaxial strain histories and parameter evolutions. Furthermore, two three-dimensional simulations are presented to give a non-homogeneous example and to demonstrate the consequences of the volume shrinkage phenomenon. As mentioned in the previous section, the current bulk modulus has always been calculated from the shear modulus evolution by assuming a constant Poisson's number $\nu = 0.35$.

8.1 Basic structures under load during cure

First, one-dimensional elastic and viscoelastic examples are considered, i.e. Eq. (13) as well as Eq. (11) together with (31) are the protagonists. In the elastic case, both a strain history and the temporal evolution of the shear modulus $\mu(t)$ have to be prescribed. For the latter an exponential saturation function as in Eq. (37) with $(\mu_0, \mu_\infty, \kappa_\mu) = (0.01\,\text{MPa}, 0.5\,\text{MPa}, 0.25\,\text{s}^{-1})$ has been used. Figure 7 also displays the applied three-phase loading that consists of a linear increase of 0.5% within the first five seconds followed by fourty seconds holding and another linear increase for five seconds.

The resulting stress evolutions versus time and strain are shown in Fig. 8. The physical observation that the cure induced stiffness increase has no impact on the stress response of a constant deformation state is correctly reproduced—as is reflected by both the constant line in the left plot and, implicitly, by the kink at 0.5% in the right hand side curve. Furthermore, the initially fast growing stiffness leads to nonlinearly increasing steps in stress during the first five seconds, whereas the behaviour is almost linear with high stiffness at the end since the saturation value has been reached meanwhile.

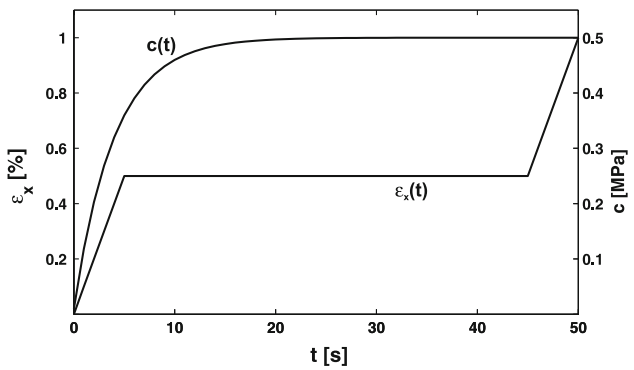

Fig. 7 3-phase strain history and temporal stiffness evolution

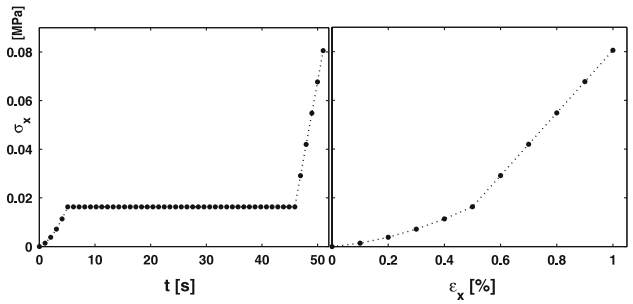

Fig. 8 Elastic stress response versus time (*left*) and strain (*right*)

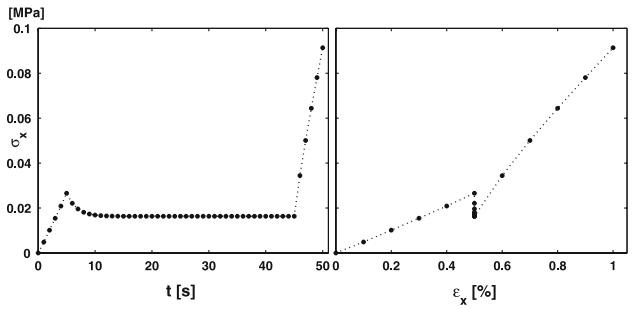

Fig. 9 Viscoelastic stress response versus time and strain

The same strain history is now applied to the viscoelastic model. While the volumetric stress coincides with that of the previous case, the isochoric part now consists of the equilibrium shear modulus evolution $\mu_\infty(t)$ and the non-equilibrium part $\mu_\star(t)$, the former being determined by the same parameters as in the elastic shear modulus evolution above. The non-equilibrium part is governed by the constant non-equilibrium shear modulus $\mu := 0.5\,\mathrm{MPa}$ and the relaxation time evolution (38) for which $(T_0, T_\infty, \kappa_\tau) = (0.025\,\mathrm{s}, 1\,\mathrm{s}, 0.25\,\mathrm{s}^{-1})$ have been chosen as parameters.

Figure 9 displays the resulting stress response versus time and strain for the viscoelastic case. Both the increase in stiffness and the stress relaxation are correctly reproduced. Note that the stress relaxes exactly to the constant value of the second loading phase of the elastic case. This behaviour is as expected because the initial relaxation times are small enough to eliminate the additional contribution of the non-equilibrium part. The superimposed relaxation process is also responsible for the straightened stress-strain curve within the first loading phase (compare right hand sides of Figs. 8 and 9), i.e. the inelastic material is less burdened due to the concurrent relaxation whereas the elastic material sustains growing stress increments due to the quickly increasing stiffness. The slightly concave shape of the final loading phase is of the same origin.

Another important aspect of curing is its influence on the viscous material properties. According to the literature [15,16] and as structurally motivated in Sects. 1.2 and 7.2, the relaxation time increases with the proceeding curing process. To visualise this effect and the stiffness gain simultaneously, the strain programme used before is now extended as depicted in Fig. 10. After two seconds of linear elongation to a strain of 2%, a holding phase lasting six seconds and another elongation follow. The simulation closes with a second holding phase and a final linear increase in strain.

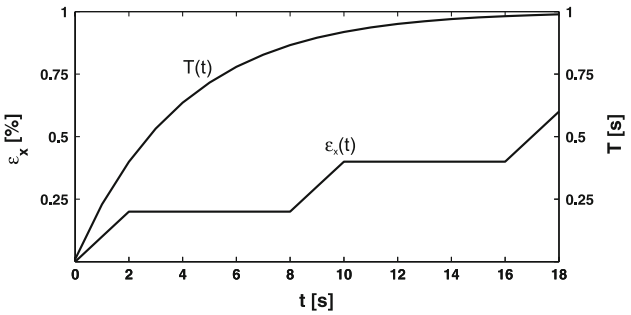

Fig. 10 5-phase strain history and relaxation time evolution

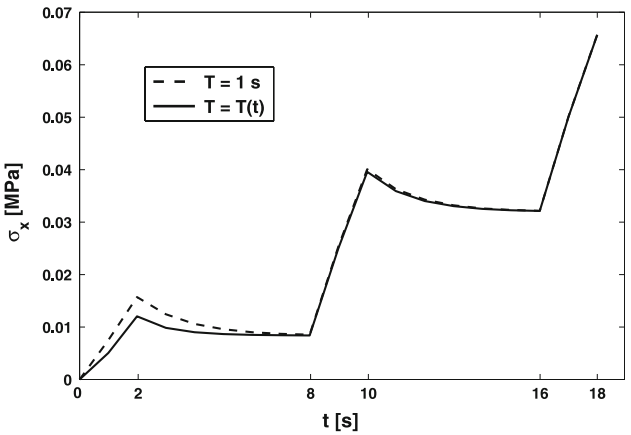

Fig. 11 Viscoelastic model: constant versus evolving relaxation time

Figure 11 compares the responses to this extended strain history for two viscoelastic materials with constant and evolving relaxation time, respectively. Thereby, the stiffness evolutions have been chosen as before, the constant relaxation time is set to be $T = 1\,\mathrm{s}$ and the relaxation time evolution, also plotted in Fig. 10, is again governed by the parameters introduced above.

As expected and physically reasonable, we observe for the material with evolving T (solid line) both a deceleration of the relaxation process from the first to the second holding phase and a smaller stress amplitude after two seconds due to the concurrent relaxation process. Since T has almost reached its saturation value—coinciding with the prescribed constant relaxation time—after 10 s (cf. Fig. 10), both materials behave virtually equal up from this point.

Finally, a three-dimensional plate with a hole in its center is considered to present an example with inhomogeneous stress distribution under load. Its dimensions are $60 \times 12 \times 2\,\mathrm{mm}^3$ and the hole has a diameter of 6 mm.

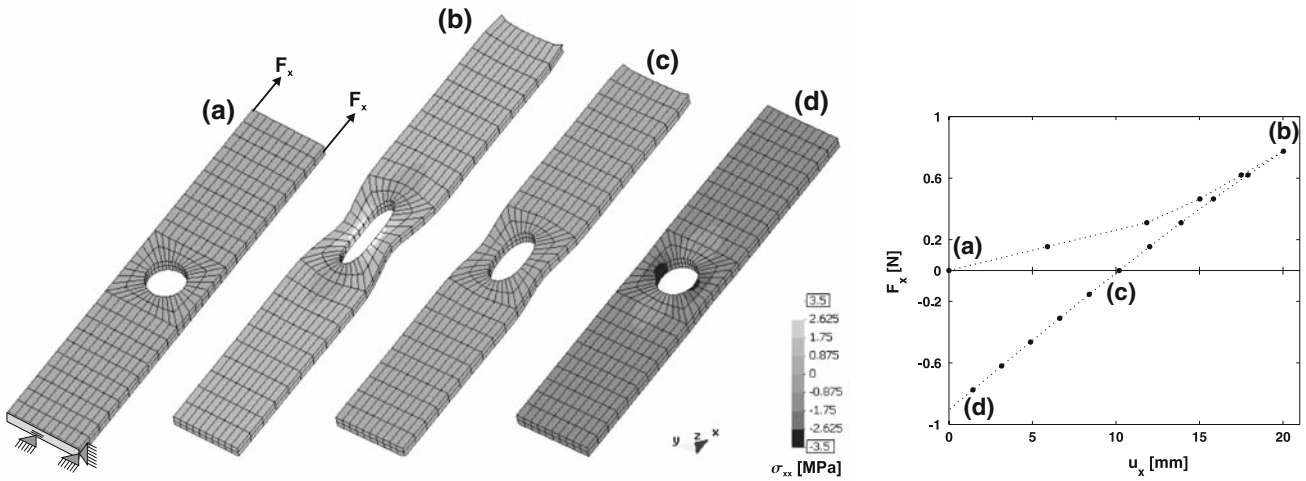

Fig. 12 Inhomogeneous 3d-example: curing plate with a centered hole, **a** initial configuration, bearing and loading, **b** deformation and stress (tensile) after five loadsteps $F_x = 0.155\,N$, **c** stress-free but deformed (due to stiffness gain) after five reverse loadsteps $F_x = -0.155\,N$, **d** nearly undeformed but compressive stresses after another five loadsteps $F_x = -0.155\,N$; load-deformation curve

The plate is discretised by 544 eight-noded hexagonal elements and mounted as depicted in Fig. 12a. Force increments of $0.155\,\mathrm{Ns}^{-1}$ are applied at the upper edge nodes to achieve elongation in x-direction. While loaded, the specimen undergoes elastic curing, whereby $(\mu_0, \mu_\infty, \kappa_\mu) = (0.001\,\mathrm{MPa}, 3.35\,\mathrm{MPa}, 0.25\,\mathrm{s}^{-1})$ have been chosen. Figure 12b–d show deformation and Cauchy stress in x-direction after different numbers of loadsteps. The first five loadsteps yield tensile stresses and a significant deformation (b). After another five loadsteps equal in magnitude but reverse in direction, the plate is stress-free but, due to the interim stiffness increase, still deformed (c). Further loadsteps into the same direction are necessary to achieve a nearly undeformed deformation, which then sustains compressive stresses (d).

8.2 Curing shrinkage

To demonstrate the shrinkage induced stress build-up during cure, a three-dimensional block, discretised by one hundred 8-noded elements, having dimensions $20 \times 7 \times 3\,\mathrm{mm}^3$ and with fixed bearing at both ends, is considered, cf. Fig. 13. The elastic model from Sect. 3, Eq. (13), again with shear modulus evolution Eq. (37) and $(\mu_0, \mu_\infty, \kappa_\mu) = (0.001\,\mathrm{MPa}, 4.0\,\mathrm{MPa}, 0.025\,\mathrm{s}^{-1})$, is applied. Thereby, the calculation of volumetric stresses is extended by a shrinkage strain as in Eq. (36) to account for the volume decrease caused by the polymerisation. As before, we assume constant Poisson number $\nu = 0.35$ and calculate the bulk modulus

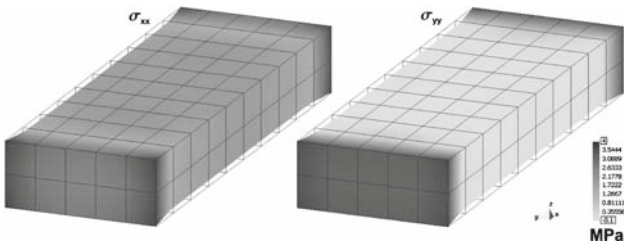

Fig. 13 Stress build-up due to curing shrinkage, Cauchy stresses in x- and y-direction after 270 min of curing

evolution from the shear modulus (40). For the evolution of the shrinkage strain $\varepsilon_s(t)$, Eq. (35) together with parameters taken from [3, p. 77], namely $(p_1, p_2, p_3, p_4, p_5, p_6) = (-1.129, 37.36\,\mathrm{min}, 1.261, -2.402, 25.74\,\mathrm{min}, 4.611)$, has been used. Figure 13 plots deformation and Cauchy stresses σ_{xx}, σ_{yy} after $t = 270\,\mathrm{min}$ of curing, indicating that significant loads can arise from the volume shrink occuring during thermoset cure.

9 Conclusion and outlook

This contribution proposes one- and three-dimensional elastic and viscoelastic material models to simulate the curing of thermoset structures undergoing small strain deformations. Based on some elementary rheological considerations the governing constitutive equations and tangent operators are derived. The numerical realisation of the models within the

finite element framework allows to simulate arbitrary structures during cure. The examples presented have proven that the developed models are suitable to correctly reproduce all the relevant phenomena observable in curing of thermosets. Nonetheless, some restrictions like the assumption of constant temperature and the purely phenomenological character of the presented approach should and will be subject to further investigations. Especially the extension towards the large strain framework is going to be dealt with in a forthcoming paper.

Acknowledgments Financial support by the Rhineland–Palatinate Graduate School 'Engineering Materials and Processes' as well as by the German Research Foundation within the collaborative project PAK 108 are gratefully acknowledged. M. Hossain is also indebted to Prof. Tobias Damm, (Department of Mathematics, University of Kaiserslautern) for fruitful discussions.

References

1. Hubert P, Johnston A, Poursartip A, Nelson K (2001) Cure kinetics and viscosity models for Hexcel 8552 epoxy resin. In: Proceedings of the 46th international SAMPE symposium. Long Beach, CA, pp 2341–2354
2. Lion A, Höfer P (2007) On the phenomenological representation of curing phenomena in contiuum mechanics. Arch Mech 59:59–89
3. Kiasat M (2000) Curing shrinkage and residual stresses in viscoelastic thermosetting resins and composites. PhD Thesis, TU Delft, Netherlands
4. Ruiz E, Trochu F (2005) Thermomechanical properties during cure of glass-polyester RTM composites: elastic and viscoelastic modeling. J Compos Mater 39:881–916
5. Ernst LJ, van't Hof C, Yang DG, Kiasat M, Zhang GQ, Bressers HJL, Caers JFJ, den Boer AWJ, Janssen J (2002) Mechanical modeling and characterization of the curing process of underfill materials. J Electron Packag 124:97–105
6. O'Brien DJ, Mather PT, White SR (2001) Viscoelastic properties of an epoxy resin during cure. J Compos Mater 35:883–904
7. Lange J (1999) Viscoelastic properties and transitions during thermal and UV cure of a methacrylate resin. Polym Eng Sci 39: 1651–1660
8. Eom Y, Boogh L, Michaud V, Sunderland P, Manson JA (2000) Time-cure-temperature superposition for the prediction of instantaneous viscoelastic properties during cure. Polym Eng Sci 40:1281–1292
9. Suzuki K, Miyano Y (1977) Change of viscoelastic properties of epoxy resin in the curing process. J Appl Polym Sci 21:3367–3379
10. Matsuoka S, Quan X, Bair HE, Boyle DJ (1989) A model for the curing reaction of epoxy resins. Macromolecules 22:4093–4098
11. White SR, Hahn HT (1992) Process modeling of composite materials: residual stress development during cure. Part I. Model formulation. J Compos Mater 26:2402–2422
12. Antonucci V, Cusano A, Giordano M, Nasser J, Nicolais L (2006) Cure-induced residual strain build-up in a thermoset resin. Compos Part A Appl Sci Manuf 37:592–601
13. Chen Y, Xia Z, Ellyin F (2001) Evolution of residual stresses induced during curing processing using a viscoelastic micromechanical model. J Compos Mater 36:522–542
14. Adolf DB, Chambers RS (2007) A thermodynamically consistent, nonlinear viscoelastic approach for modeling thermosets during cure. J Rheol 51:23–50
15. Hojjati M, Johnston A, Hoa SV, Denault J (2004) Viscoelastic behaviour of Cytec FM73 adhesive during cure. J Appl Polym Sci 91:2548–2557
16. Kim YK, White SR (1996) Stress relaxation behaviour of 3501-6 epoxy resin during cure. Polym Eng Sci 36:2852–2862
17. Thomas R, Durix S, Sinturel C, Omonov T, Goossens S, Groeninckx G, Moldenaers P, Thomas S (2007) Cure kinetics, morphology and miscibility of modified DGEBA-based epoxy resin - effects of a liquid rubber inclusion. Polymer 48:1695–1710
18. Han HG, Kim WG, Yoon HG, Moon TJ (1998) Curing reaction of biphenyl epoxy resin with different phenolic functional hardeners. J Polym Sci Part A Polym Chem 36:773–783
19. Karkanas PI, Partridge IK (1996) Modelling the cure of a commercial epoxy resin for applications in resin transfer moulding. Polym Int 41:183–191
20. van't Hof C (2006) Mechanical characterization and modeling of curing thermosets. PhD Thesis, TU Delft, Netherlands
21. Adolf DB, Martin JE (1996) Calculation of stresses in crosslinking polymers. J Compos Mater 30:13–34
22. Adolf DB, Chambers RS (1997) Verification of the capability for quantitative stress prediction during epoxy cure. Polymer 38:5481–5490
23. Adolf DB, Martin JE, Chambers RS, Burchett SN, Guess TR (1998) Stresses during thermoset cure. J Mater Res 13:530–550
24. Adolf DB, Chambers RS, Caruthers JM (2004) Extensive validation of a thermodynamically consistent, nonlinear viscoelastic model for glassy polymers. Polymer 45:4599–4621
25. Haupt P, Lion A (2002) On finite linear viscoelasticity of incompressible isotropic materials. Acta Mech 159:87–124
26. Lion A (1998) Thixotropic behaviour of rubber under dynamic loading histories: experiments and theories. J Mech Phys Solids 46:895–930
27. Lion A (1997) On the large deformation behaviour of reinforced rubber at different temperatures. J Mech Phys Solids 45:1805–1834
28. Gillen KT (1988) Effect of cross-links which occur during continuous chemical stress-relaxation. Macromolecules 21:442–446
29. Simo JC, Hughes TJR (1998) Computational inelasticity. Springer, New York
30. Hill RR, Muzumdar SV, Lee LJ (1995) Analysis of volumetric changes of unsaturated polyester resins during curing. Polym Eng Sci 35:852–859
31. Simon SL, McKenna GB, Sindt O (2000) Modeling the evolution of the dynamic mechanical properties of a commercial epoxy resin during cure after gelation. J Appl Polym Sci 76:495–508